



CHORUS

This is the accepted manuscript made available via CHORUS. The article has been published as:

Direct measurement of the spin gap in a quasi-one-dimensional clinopyroxene: $\text{NaTiSi}_2\text{O}_6$

Harlyn J. Silverstein, Alison E. Smith, Cole Mauws, Douglas L. Abernathy, Haidong Zhou, Zhiling Dun, Johan van Lierop, and Christopher R. Wiebe

Phys. Rev. B **90**, 140402 — Published 13 October 2014

DOI: [10.1103/PhysRevB.90.140402](https://doi.org/10.1103/PhysRevB.90.140402)

Direct measurement of the spin gap in a quasi-one dimensional clinopyroxene: $\text{NaTiSi}_2\text{O}_6$

Harlyn J. Silverstein,¹ Alison E. Smith,² Cole Mauws,² Douglas L. Abernathy,³
Haidong Zhou,^{4,5} Zhiling Dun,⁴ Johan van Lierop,⁶ and Christopher R. Wiebe^{1,2,7}

¹*Department of Chemistry, University of Manitoba, Winnipeg R3T 2N2, Canada*

²*Department of Chemistry, University of Winnipeg, Winnipeg R3B 2E9, Canada*

³*Quantum Condensed Matter Division, Oak Ridge National Laboratory, Oak Ridge 37831-6475, United States*

⁴*Department of Physics and Astronomy, University of Tennessee-Knoxville, Knoxville 37996-1220, United States*

⁵*National High Magnetic Field Laboratory, Florida State University, Tallahassee 32306-4005, United States*

⁶*Department of Physics and Astronomy, University of Manitoba, Winnipeg R3T 2N2, Canada*

⁷*Department of Physics and Astronomy, McMaster University, Hamilton L8S 4M1, Canada*

(Dated: September 9, 2014)

True inorganic Spin-Peierls materials are extremely rare, but $\text{NaTiSi}_2\text{O}_6$ was at one time considered an ideal candidate due to it having well separated chains of edge-sharing TiO_6 octahedra. At low temperatures, this material undergoes a phase transition from $C2/c$ to $P\bar{1}$ symmetry, where Ti^{3+} - Ti^{3+} dimers begin to form within the chains. However, it was quickly realized with magnetic susceptibility that simple spin fluctuations do not progress to the point of enabling such a transition. Since then, considerable experimental and theoretical endeavours have been taken to find the true ground state of this system and explain how it manifests. Here, we employ the use of x-ray diffraction, neutron spectroscopy, and magnetic susceptibility to directly and simultaneously measure the symmetry loss, spin singlet-triplet gap, and phonon modes. A gap of 53(3) meV was observed, fit to the magnetic susceptibility, and compared to previous theoretical models to unambiguously assign $\text{NaTiSi}_2\text{O}_6$ as having an orbital-assisted Peierls ground state.

Electrons have charge, orbital and spin degrees of freedom. However, the coupling between these degrees of freedom and to the lattice can result in new, exotic and fascinating avenues for physicists to explore. $\text{NaTiSi}_2\text{O}_6$ clinopyroxene is a Mott insulator quasi-one dimensional Ti^{3+} system that crystallizes in the monoclinic space group $C2/c$. Two aspects of this material are quite intriguing: 1) Chains of slightly distorted TiO_6 octahedra are skew-edge connected and are well separated by SiO_4 layers (Figure 1)^{1,2} and 2) unlike Cu^{2+} , which is a spin-1/2 $3d^9$ ion, Ti^{3+} is a spin-1/2 $3d^1$ ion. The zig-zag chains result from the overlapping of nearly degenerate xy and yz orbitals (xz orbitals are inert^{4,5}). Ignoring spin, the lower energy t_{2g} orbitals split into a doublet and higher energy singlet and remain far removed from the e_g orbitals resulting from crystal-field splitting (Figure 1). Consequently, these combined effects mean that super exchange interactions are enhanced on account of the low spin-number while the Jahn-Teller effect is suppressed due to the ordering of nearly degenerate lower energy orbitals as opposed to higher energy ones⁶.

Previous experiments on $\text{NaTiSi}_2\text{O}_6$ have been numerous^{1-5,7-10}. A broad feature appearing in the magnetic susceptibility and heat capacity at 210 K indicates a phase transition typical of Spin-Peierls materials, but the transition occurs at higher temperatures than predicted by the Bonner-Fisher equation². This implies that simple magnetic fluctuations are not strong enough to induce spin-pairing. On the other hand, it was noticed that Ti^{3+} dimerization occurs as the system transitions from $C2/c$ to the $P\bar{1}$ space group at lower temperatures with no new magnetic Bragg peaks^{2,3,7,10}. Raman and infrared spectroscopy show broadness in the phonon frequencies that

split and sharpen not only as the temperature is lowered, but also as Ti^{3+} is substituted for higher spin ions like V^{3+} and Cr^{3+8} . This implies that the orbitals do indeed play a special role in this material, leading Popović *et al.* to conclude that this system transitions from a dynamical Jahn-Teller phase into an orbitally ordered phase.

A microscopic model based on symmetry-constrained hopping terms was first introduced by Konstantinović *et al.*^{4,5} and was later expanded upon by Hikiyama and Motome^{6,11}. Using these models, it was shown that the Jahn-Teller effect is suppressed and the ground states are predicted to be either spin-antiferromagnetic/ferroorbital or spin-ferromagnetic/antiferroorbital based on the relative strength of the Hund's rule coupling parameter. Alternatively, Popović *et al.*¹² predicted a spin-1 Haldane chain ground state using Density Functional Theory, although the accuracy of their approach was later questioned¹³. Other studies by Shiraka *et al.*¹⁴ and van Wezel and van den Brink^{15,16} found that spin-orbital fluctuations actually drive the system through an Orbital-Peierls transition; neglecting them results in an alternating ferromagnetically correlated ground state.

This communication seeks to clarify experimentally the ground state through the use of x-ray scattering, neutron spectroscopy and magnetic susceptibility. We show unambiguously and simultaneously the detection of the singlet-triplet gap and phonon modes previously ascribed to orbital ordering through the transition^{4,5}. The magnetic susceptibility is then fit to the true gap and compared to theoretical predictions. Powder $\text{NaTiSi}_2\text{O}_6$ samples were prepared through a method described previously². Temperature-dependent x-ray diffraction

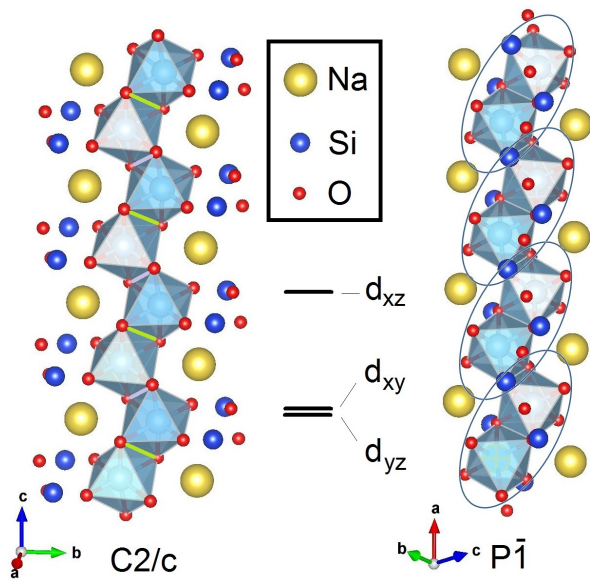


FIG. 1. The skew-edged TiO_6 octahedra in the monoclinic phase (left) at $T=300$ K and triclinic phase (right) at $T=15$ K. The unit cells used for the refinement are from Redhammer *et al.*³. In the monoclinic phase, all Ti^{3+} - Ti^{3+} distances are equivalent and the connected skew-edges have been coloured green and violet for clarity. For the triclinic phase chain, the Ti^{3+} - Ti^{3+} dimerization is depicted with an oval. The complete unit cell in both phases has been omitted for clarity. A schematic of the splitting of the t_{2g} orbitals is presented in the centre with the z -direction defined as the principal axis of the TiO_6 octahedron and the approximate chain length direction.

measurements were made using a Brüker D8 Discover diffractometer using a Göbel mirror and a low temperature sample stage with a closed-cycle refrigerator. Neutron spectroscopy on the polycrystalline sample was performed on ARCS¹⁷ at the Spallation Neutron Source (Oak Ridge, TN) using a closed cycle refrigerator and incident neutron energies of 100 and 200 meV. An aluminum can containing two grams of sample was used. Data was compiled using MantidPlot¹⁸ and analyzed using the DAVE package¹⁹. The magnetic susceptibility was measured with a Vibrating Sample Magnetometer (VSM) option on a Physical Property Measurement System (Quantum Design) using an applied field of 0.1 T.

The experimental studies on $\text{NaTiSi}_2\text{O}_6$ are often limited by the availability of sample. A high-pressure method¹ has been known to yield small single crystals suitable for x-ray diffraction, but not neutron spectroscopy. The structural model of Redhammer *et al.*³ was used for the refinement of our powder sample (not shown) and no deviations in the lattice parameters or atomic coordinates were found within error. While Redhammer *et al.* observed a sharp structural transition at 197 K³, Ninomiya *et al.*⁷ found a gradual splitting of the Ti^{3+} - Ti^{3+} distances that begin to develop below 210 K. To address the discrepancy, temperature dependent x-ray diffraction

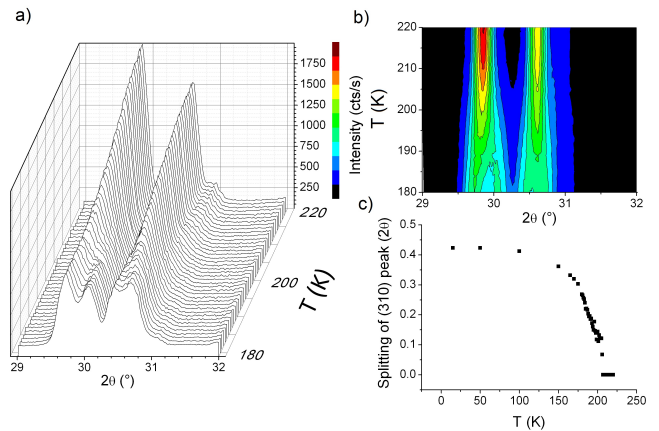


FIG. 2. **a)** Waterfall and **b)** contour plots showing the broadening of the $(\bar{2}21)$ and (331) peaks on the left and right respectively as the temperature is lowered from 220 to 180 K, which split in a predictable fashion **c)** at the critical temperature. The colour bar in **b)** is normalized to the intensities in **a)**

was performed between 220 K and 180 K in 1 K steps (temperature was stable to within 0.1 K). The system was allowed to equilibrate for half an hour at each temperature. It was found that a reproducible broadening of the most intense monoclinic peaks ($(\bar{2}21)$ and (310)) begins to occur below 212 K with accompanying splitting by 196 K (Figures 2a and b). The $(\bar{2}21)$ peak splits into the (102) left-moving and (120) right-moving peaks while the (310) peak splits into the (012) left-moving and (021) right-moving peaks in 2θ . The peaks continue to split in a predictable fashion with temperature (Figure 2c), until the (120) and (012) peaks merge when the splitting is maximal at low temperature (not shown). However, the split itself causes a discontinuous jump in the Ti^{3+} - Ti^{3+} distances. These results appear to be intermediate to those of Redhammer *et al.* and Ninomiya *et al.* While this could be due either to the formers use of a single crystal or to the latters lack of resolution, a more likely scenario is that the results from Ninomiya *et al.* are a direct consequence of a different choice of triclinic unit cell with two distinct Ti^{3+} sites. Figure 2c does present researchers with an avenue of obtaining an order parameter similar to the case of CuGeO_3 ^{20–23}. For $\text{NaTiSi}_2\text{O}_6$, obtaining such an order parameter is difficult since no new crystal or magnetic Bragg peaks have been detected through the transition temperature while the symmetry of the unit cell dramatically changes. One must be extremely careful when making these measurements: single crystals of high-purity are required to obtain the correct order parameter since a powder can result in a broadening of the transition temperature²².

Many attempts have been made to extract and calculate the size of the singlet-triplet gap of the ordered domains. Isobe *et al.* estimated it to be 500 K from magnetic susceptibility². Baker *et al.* found gap sizes of

700(100) and 595(7) K from muon spectroscopy and magnetic susceptibility measurements respectively¹⁰ while Hikihara and Motome estimated gaps between 638 and 665 K for different Hund's coupling strengths^{6,11}. Time-of-flight neutron spectroscopy provides a more direct avenue to measure the energy gap. In a time-of-flight experiment, neutrons of certain energy E_i are selected and made incident on the sample. A bank of detectors surrounds the sample and the time it takes for the neutron to travel from the sample to the detector is recorded. The relative energy transfer between the sample and the incident neutron are obtained by comparing the actual neutron traveling time relative to the speed of a neutron with incident energy E_i . Using such a procedure on ARCS, it is possible to obtain both the elastic and inelastic profiles of the material as a function of Q (\AA^{-1}). Neutron spectroscopy has the additional benefit of providing direct experimental evidence of the spin gap by taking advantage of the neutron's magnetic moment—that is, once the magnetic component of the scatter is isolated, the gap can be qualitatively observed before more quantitative fits are implemented²⁴. Neutrons also have energies comparable to phonons in real materials. Therefore, the phase transition observed with diffraction, the phonon modes detected from Raman spectroscopy, and the spin gap may be obtained *simultaneously* on a single sample.

The intensity detected has three primary components: a background term due to scattering from the sample environment, the phonon component, and the magnetic component. The background term can be removed by measuring the intensity of an empty aluminum can run at each temperature. The phonon and magnetic components can then be isolated from each other by subtracting a phonon-dominated high temperature data set from the low temperature data set where the magnetic contribution is larger. The results are shown in Figures 3a and b where 12 hour-long background-corrected data sets from 300 K have been subtracted from data sets at 50 K. A cut and Lorentzian fit of the excitation on top of a linear background was used to estimate the error. A clear increase in intensity is observed at low Q at 53(3) meV, while intense regions at high Q are observed at about 110, 120, and 130 meV. Magnetic excitations tend to decrease in the intensity with increasing Q as dictated by the magnetic form factor for Ti^{3+} while phonon modes increase in intensity with higher Q . The 53 and 130 meV excitations are compared to the Ti^{3+} magnetic form factor in Figure 3c and can be unambiguously assigned to a magnetic and a phonon mode respectively (addressed later) occurring below the transition. The width of the magnetic excitation is instrument resolution limited and is 3-4% of the incident energy. For TiOBr ²⁴, a Bose correction factor was applied to see the gap more clearly. This could not be done here due to the additional change in phonon modes that occurs as the temperature is lowered that blends with the magnetic scatter.

An excitation of 53(3) meV equates to $\Delta/k_B=650(40)$ K, which precisely agrees with calculations from Hiki-

hara and Motome⁶. This would assign $\text{NaTiSi}_2\text{O}_6$ with a Hund's coupling of approximately 0.10, which has an accompanying exchange energy of 250 K, gyromagnetic ratio of 1.87, and Jahn-Teller stabilization energy of 90 K. This gap may be compared to other similar systems such as TiOBr ($\Delta/k_B \approx 250$ K, $J=364$ K), TiOCl ($\Delta/k_B \approx 430-440$ K, $J=660-676$ K), CuGeO_3 ($\Delta/k_B \approx 25$ K)²⁴, and recently TiPO_4 ($\Delta/k_B \approx 350$ K)^{25,26}. The width of the present transition is quite sharp compared to CuGeO_3 in particular. This is likely due to the non-negligible role of highly extended and anisotropic d -orbitals within $\text{NaTiSi}_2\text{O}_6$ that influence the zig-zagged chain structure^{2,4,5}. Further credence to this mechanism is given when this material is compared to other potential Orbital-Peierls materials such as MgTi_2O_4 ²⁷⁻²⁹. Although MgTi_2O_4 adopts a spinel structure, orbitals direct the flow of electrons along one-dimensional paths that lead to a dimer state in this material accompanying a metal-insulator transition below approximately 260 K. The difference between this material and $\text{NaTiSi}_2\text{O}_6$ is that the one-dimensional chains are more obvious here; the effects of chemical substitution and doping on the one-dimensionality of the system can be systematically explored⁸.

Figure 3d shows the magnetic susceptibility of $\text{NaTiSi}_2\text{O}_6$ with a Curie-law correction at low temperatures used to correct for the susceptibility or unpaired "stray" spins². The susceptibility was measured between 2 and 350 K. The Curie-law correction appears to fail at temperatures lower than 30 K as compared to the original susceptibility measurements made by Isobe *et al.*². This is most likely due to their use of a Superconducting Quantum Interference Device (SQUID) magnetometer, which is far more sensitive than a VSM. The magnetic susceptibility was fit to the following equation²:

$$\chi = \alpha e^{-\Delta/(kT)} + \chi_0 \quad (1)$$

where α is a scaling constant indicative of the dispersion of the gap, Δ , k , and T are the gap energy, Boltzmann constant and temperature respectively, and χ_0 are the remaining contributions to the susceptibility including the diamagnetic and Van Vleck paramagnetism components. Only α and χ_0 were allowed to vary in the region between 210 K and 50 K, where the final fit yielded values of $9.30(2) \times 10^{-3}$ and 4.25×10^{-5} emu/mol respectively. The fit differs only slightly from Isobe *et al.*² and is quite good considering that the gap energy was kept fixed.

If orbitals do play a role in the magnetism, then they should exhibit critical phenomena with similar temperature dependence accompanying the magnetic transition. Such an effect has been observed previously using Raman and infrared spectroscopy^{4,5,8,9}, where it was shown that broad phonon modes sharpen not only as the temperature is lowered through the phase transition, but also as more electrons are placed onto the t_{2g} orbitals using chemical substitution. These modes can also be detected using neutron spectroscopy and are shown in Figure 4, although the resolution of the instrument is not high

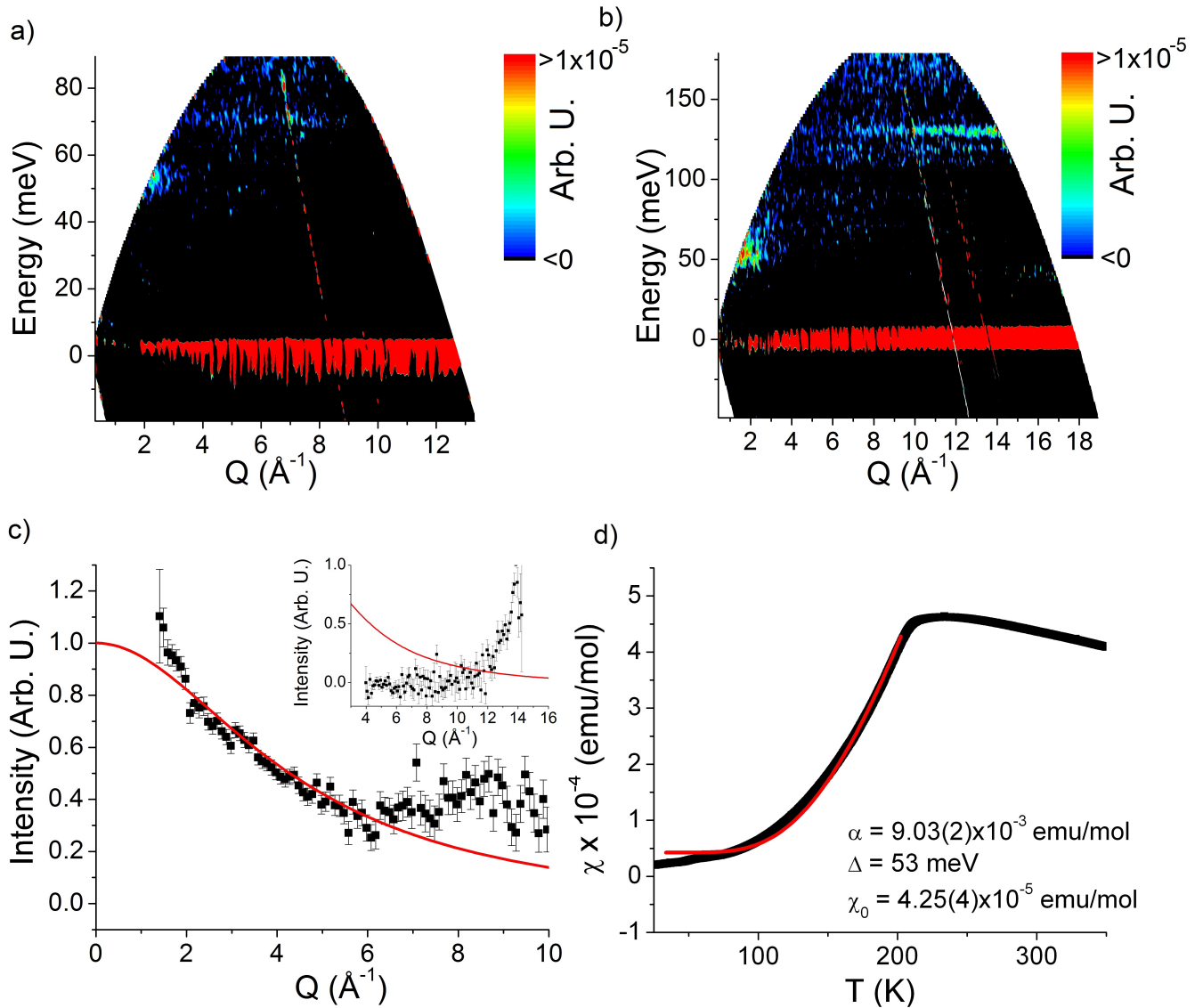


FIG. 3. Neutron spectroscopy data treated with the methods described in the text using incident energies of a) 100 and b) 200 meV. Only positive intensities are shown; c) A cut of the magnetic excitation (outset) over [48, 58] meV was renormalized and compared to the Ti^{3+} magnetic form factor (red line). The increase in intensity appearing above 7 \AA^{-1} is due to phonons that cannot be subtracted from the rest of the data. The inset shows a similar comparison using a phonon integrated over [125, 135] meV; d) The Curie-law was subtracted from the DC magnetic susceptibility (black) to correct for the presence of stray spins due to defects. The data has been fit with the equation described within the text (red).

enough to detect the phonon softening observed using Raman^{4,5}. Almost all of the predicted phonon modes within the a_{1g} irreducible representation are detected both above and below the transition in addition to the mode-sharpening as the temperature is lowered, which can indicate bond disorder^{8,9} at high temperatures. This picture agrees with the x-ray diffraction measurements of Figure 2 where the peaks begin to broaden as the temperature is lowered until the split. x-ray diffraction is an elastic process, but an increase in the peak width indicates that the domain sizes are shrinking, which can be accounted for by bond disorder due to orbital fluc-

tuations. Konstantinović *et al.*⁴ were able to observe a temperature dependence of the full width at half maximum of these phonon modes that increases with lowering temperature until the transition.

To summarize, powder $\text{NaTiSi}_2\text{O}_6$ was prepared and characterized using x-ray diffraction, time-of-flight neutron spectroscopy and magnetic susceptibility. The spin singlet-triplet gap of 53 meV was directly detected at low temperatures accompanying changes in the phonon spectrum. Using this gap, the magnetic susceptibility could be fit after subtraction of a low-temperature Curie-like feature. The value of the gap precisely agrees with the-

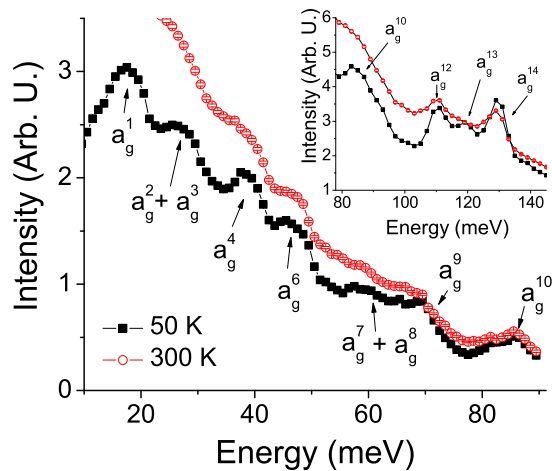


FIG. 4. Phonon modes detected using inelastic neutron scattering. Only the modes below the transition are labeled for clarity. Error bars are smaller than the symbols.

oretical predictions (Hikihara and Motome^{6,11} in particular) and unambiguously shows that $\text{NaTiSi}_2\text{O}_6$ adopts an an orbital-assisted Peierls ground state.

ACKNOWLEDGMENTS

The authors would like to acknowledge support from NSERC, CFI, and the ACS Petroleum fund. HJS graciously thanks support from the Vanier CGS and the MGS, as well as R Desautels for assisting with the instrumentation. AES and CM wish to thank support from the NSERC USRA program. ZLD and HDZ are supported by NSF-DMR-1350002 while CRW thanks the CRC program (Tier II). A portion of this research at Oak Ridge National Laboratory's Spallation Neutron Source was sponsored by the Scientific User Facilities Division, Office of Basic Energy Sciences, U.S. Department of Energy.

- ¹ H. Ohashi, T. Fujita, and T. Osawa, *J. Japan. Assoc. Min. Petr. Econ. Geol.* **77**, 305 (1982).
- ² M. Isobe, E. Ninomiya, A. N. Vasil'ev, and Y. Ueda, *J. Phys. Soc. Jpn.* **71**, 1423 (2002).
- ³ G. J. Redhammer, H. Ohashi, and G. Roth, *Acta. Cryst. B* **59**, 730 (2003).
- ⁴ M. J. Konstantinović, J. van den Brink, Z. V. Popović, V. V. Moshchalkov, M. Isobe, and Y. Ueda, *J. Magn. Magn. Mater.* **272-276**, e657 (2004).
- ⁵ M. J. Konstantinović, J. van den Brink, Z. V. Popović, V. V. Moshchalkov, M. Isobe, and Y. Ueda, *Phys. Rev. B* **69**, 020409(R) (2004).
- ⁶ T. Hikihara and Y. Motome, *Phys. Rev. B* **70**, 214404 (2004).
- ⁷ E. Ninomiya, M. Isobe, Y. Ueda, M. Nishi, K. Ohoyama, H. Sawa, and T. Ohama, *Physica B* **329-333**, 884 (2004).
- ⁸ Z. V. Popović, M. J. Konstantinović, Z. D. Cević Mitrović, M. Isobe, and Y. Ueda, *Physica B* **378-380**, 1072 (2006).
- ⁹ Z. V. Popović, M. J. Konstantinović, V. N. Popov, A. Cantarero, Z. Dohčević-Mitrović, M. Isobe, and Y. Ueda, *Phys. Rev. B* **71**, 224302 (2005).
- ¹⁰ P. J. Baker, S. J. Blundell, F. L. Pratt, T. Lancaster, M. L. Brooks, W. Hayes, M. Isobe, Y. Ueda, M. Hoinkis, M. Sing, M. Klemm, S. Horn, and R. Claessen, *Phys. Rev. B* **75**, 094404 (2007).
- ¹¹ T. Hikihara and Y. Motome, (2004), arXiv:cond-mat/0410411v1.
- ¹² Z. S. Popović, Ž. V. Šljivančanin, and F. R. Vukajlović, *Phys. Rev. Lett.* **93**, 036401 (2004).
- ¹³ S. V. Streltsov, O. A. Popova, and D. I. Khomskii, *Phys. Rev. Lett.* **96**, 249701 (2006).
- ¹⁴ T. Shirakawa, Y. Ohta, and T. Mizokawa, *Physica B* **378-380**, 1056 (2006).
- ¹⁵ J. van Wezel and J. van den Brink, *J. Magn. Magn. Mater.* **290-291**, 318 (2005).
- ¹⁶ J. van Wezel and J. van den Brink, *Europhys. Lett.* **75**, 957 (2006).
- ¹⁷ D. L. Abernathy, M. B. Stone, M. J. Logiullo, M. S. Lucas, O. Delaire, X. Tang, J. Y. Y. Lin, and B. Fultz, *Rev. Sci. Instrum.* **83**, 015114 (2012).
- ¹⁸ M. Project, "Mantid: Manipulation and analysis toolkit for instrument data,".
- ¹⁹ R. T. Azuah, L. R. Kneller, Y. Qiu, P. L. W. Tregenna-Piggott, C. M. Brown, J. R. D. Copley, and R. M. Dimeo, *J. Res. Natl. Inst. Stan. Technol.* **114**, 341 (2009).
- ²⁰ M. D. Lumsden, B. D. Gaulin, H. Dabkowska, and M. L. Plumer, *Phys. Rev. Lett.* **76**, 4919 (1996).
- ²¹ M. D. Lumsden, B. D. Gaulin, and H. Dabkowska, *Phys. Rev. B* **57**, 14097 (1998).
- ²² M. D. Lumsden, B. D. Gaulin, and H. Dabkowska, *Phys. Rev. B* **58**, 12252 (1998).
- ²³ S. Haravifard, K. C. Rule, H. A. Dabkowska, B. D. Gaulin, Z. Yamani, and W. J. L. Buyers, *J. Phys. Condens. Matter* **19**, 436222 (2007).
- ²⁴ J. P. Clancy, B. D. Gaulin, C. P. Adams, G. E. Granroth, A. I. Kolesnikov, T. E. Sherline, and F. C. Chou, *Phys. Rev. Lett.* **106**, 117401 (2011).
- ²⁵ M. Bykov, J. Zhang, A. Schönleber, A. Wölfel, S. I. Ali, S. van Smaalen, R. Glaum, H.-J. Koo, M.-H. Whangbo, P. G. Reuvekamp, J. M. Law, C. Hoch, and R. K. Kremer, *Phys. Rev. B* **88**, 184420 (2013).
- ²⁶ D. Wulferding, A. Möller, K.-Y. Choi, Y. G. Pashkevich, R. Y. Babkin, K. V. Lamonova, P. Lemmens, J. M. Law, R. K. Kremer, and R. Glaum, *Phys. Rev. B* **88**, 205136 (2013).
- ²⁷ S. Leoni, A. N. Yaresko, N. Perkins, H. Rosner, and L. Craco, *Phys. Rev. B* **78**, 125105 (2008).
- ²⁸ S. V. Streltsov and D. I. Khomskii, *Phys. Rev. B* **89**, 161112(R) (2014).
- ²⁹ D. I. Khomskii and T. Mizokawa, *Phys. Rev. Lett.* **94**, 156402 (2005).